The Astrophysical Journal, 723:89–99, 2010 November 1 doi:10.1088/0004-637X/723/1/89

WAVELENGTH CALIBRATION OF THE VLT-UVES SPECTROGRAPH

Jonathan B. Whitmore[1], Michael T. Murphy[2], and Kim Griest[1]
[1] Department of Physics, University of California, San Diego, CA 92093, USA; jonathan.b.whitmore@gmail.com, mmurphy@swin.edu.au, kgriest@ucsd.edu
[2] Centre for Astrophysics and Supercomputing, Swinburne University of Technology, Melbourne, Victoria 3122, Australia
Received 2010 April 12; accepted 2010 August 25; published 2010 October 7

ABSTRACT

We attempt to measure possible miscalibration of the wavelength scale of the VLT-UVES spectrograph. We take spectra of QSO HE0515-4414 through the UVES iodine cell which contains thousands of well-calibrated iodine lines and compare these lines to the wavelength scale from the standard thorium–argon pipeline calibration. Analyzing three exposures of this $z = 1.71$ QSO, we find two distinct types of calibration shifts needed to correct the Th/Ar wavelength scale. First, there is an overall average velocity shift of between 100 m s^{-1} and 500 m s^{-1} depending upon the exposure. Second, within a given exposure, we find intra-order velocity distortions of 100 m s^{-1} up to more than 200 m s^{-1}. These calibration errors are similar to, but smaller than, those found earlier in the Keck HIRES spectrometer. We discuss the possible origins of these two types of miscalibration. We also explore the implications of these calibration errors on the systematic error in measurements of $\frac{\Delta\alpha}{\alpha}$, the change in the fine-structure constant derived from measurement of the relative redshifts of absorption lines in QSO absorption systems. The overall average, exposure-dependent shifts should be less relevant for fine-structure work, but the intra-order shifts have the potential to affect these results. Using either our measured calibration offsets or a Gaussian model with sigma of around 90 m s^{-1}, Monte Carlo mock experiments find errors in $\frac{\Delta\alpha}{\alpha}$ of between $1 \times 10^{-6} N_{\rm sys}^{-1/2}$ and $3 \times 10^{-6} N_{\rm sys}^{-1/2}$, where $N_{\rm sys}$ is the number of systems used and the range is due to dependence on how many metallic absorption lines in each system are compared.

Key words: atomic data – cosmological parameters – instrumentation: spectrographs – quasars: absorption lines – techniques: spectroscopic

Online-only material: color figures

1. INTRODUCTION

In a recent paper (Griest et al. 2010), it was shown that Keck HIRES spectrograph measurements of absorption features in high redshift QSOs calibrated with the normal thorium–argon (Th/Ar) technique contained overall average velocity shifts between exposures of up to 2000 m s^{-1} over several nights and calibration errors of up to 500 m s^{-1} even within a single echelle order in a single exposure. Similar wavelength calibration problems were found previously by Osterbrock et al. (2000) and Suzuki et al. (2003). These results were found by recalibrating the wavelength scale using spectra taken through the Keck HIRES iodine cell. The iodine cell, which has been used extensively in the Doppler method search for extrasolar planets, puts several sharp lines per Angstrom on top of the QSO spectrum, and its reproducible absorption spectrum allows extrasolar planet workers to attain a relative velocity precision of around 5 m s^{-1} between exposures taken up to several years apart (Johnson et al. 2006; Konacki 2009). The analysis in Griest et al. (2010) compared the iodine cell wavelength calibration to Th/Ar calibration with two separate Keck HIRES analysis pipelines (XIDL and MAKEE) and so is probably measuring calibration problems with the Th/Ar calibration of the spectrograph itself rather than problems just with the standard calibration software.

For most astronomical work, wavelength calibration errors of around 1 km s^{-1} are not important, but over the past few years several groups have used absorption lines in the spectra of high redshift QSOs to measure or place limits on possible changes in the fine-structure constant over cosmological time. There has been considerable controversy in experimental measurements of $\frac{\Delta\alpha}{\alpha}$ using high redshift absorption systems, with claims of detection and also limits on variation inconsistent with those claims. See Murphy et al. (2008) for a summary.

If the fine-structure constant was different 10 billion years ago by the claimed detection of $\frac{\Delta\alpha}{\alpha} = (-5.7 \pm 1.1) \times 10^{-6}$ (Murphy et al. 2003, 2004), relative atomic transition wavelengths are expected to differ from their lab values by up to $\sim$200 m s^{-1}. For such experimental uses, it is important to pay careful attention to calibration errors of the size reported above. However, it is important to understand that while individual measurement errors may be larger than the expected signal, if many atomic transitions are used in many QSO absorption systems, it may be possible to average away these calibration uncertainties. See, for example, Murphy et al. (2009).

The results of Griest et al. (2010) apply only to the Keck HIRES instrument, but there is another instrument, the VLT-UVES spectrograph, that is playing a key role in the search for possible changes in the fine-structure constant using absorption lines in high redshift QSOs. In this paper, we perform a similar recalibration of the standard UVES Th/Ar wavelength calibration pipeline using the VLT iodine cell. We find similar, but smaller, wavelength calibration errors than found in HIRES. We discuss the possible origin of these offsets, in particular whether they arise from the UVES pipeline software or systematic errors within the telescope and/or spectrograph. We also make a first attempt at calculating whether these calibration errors can give rise to important systematic errors in the measurements to date of $\frac{\Delta\alpha}{\alpha}$.

2. OBSERVATIONS

Six exposures were taken of the quasar HE0515-4414 ($z = 1.71$, $V \approx 14.9$ mag) with the VLT-UVES spectrograph in 2003 October. In this paper, we analyze the wavelength calibration of the three exposures that were taken with the iodine cell in place. We include a journal of these observations in Table 1. Over the wavelength range of interest, the median signal/noise of

Table 1
Journal of Observations

Exposure and Date	Time (UT)	Th/Ar Time (UT)
1 2003 Oct 11	07:32	10:56
2 2003 Oct 11	08:13	10:56
3 2003 Oct 13	05:31	07:06

the spectra extracted from these exposures is around 20 pixel^{-1} for the upper "u" chip and around 11 pixel^{-1} for the lower "l" chip. One pixel corresponds to about 1.5 km s^{-1} at the leading edge of each echelle order and around 0.9 km s^{-1} at the trailing edge. We note that ESO's specifications for UVES are that the gratings, after being moved, be returned to the same position to within a tolerance corresponding to 0.1 pixels (D'Odorico et al. 2000). Thus, naively, we might expect to see an overall non-zero velocity calibration shift between the iodine and Th/Ar lines of roughly 140 m s^{-1} at 5500 Å. The six QSO exposures were taken during two nights, with the first two I_2 QSO exposures being taken on the first night and the third I_2 exposure taken on the next. The first two exposures were calibrated with the same Th/Ar exposure; however, we note that the gratings were moved after the two data exposures and then moved back to the same position in order to take the Th/Ar exposure. The third I_2 QSO exposure was followed first by a non-I_2 QSO exposure (same QSO, grating setting, etc.) and then by the Th/Ar calibration exposure. We had hoped this scheduling would remove a possible source of error caused by grating movement, but in fact, the third QSO I_2 exposure was part of a different "observation block," meaning the gratings were reset (moved and then returned) between the data and Th/Ar exposures. We therefore expect overall velocity shifts between the I_2 and Th/Ar wavelength scales of order 140 m s^{-1} for all three of our QSO exposures through the I_2 cell.

We can also estimate an overall average velocity shift having to do with the position of the QSO in the spectrograph slit. The slit width is 0.″7 and our exposures were taken with seeing between 0.″65 and 0.″85. This slit-width projects onto the CCD with an FWHM of about 4.8 km s^{-1} ($R \sim 62{,}000$). Therefore, if a given exposure has, for example, a 0.″1 positioning error, we might expect a roughly 600 m s^{-1} overall calibration shift, substantially larger than the error caused by the resetting of the spectrometer grating.

In more detail, we note that each 2400 s I_2 exposure used only the red arm of UVES in the standard 600 nm central wavelength setting for I_2 observations. The red arm of UVES has a detector containing two CCD detectors covering the wavelength ranges 496–597 and 599–707 nm. No on-chip binning was used; the pixels have a width of $\approx$1.3 km s^{-1}, providing $\approx$3.7 pixels per FWHM resolution element. A circular baffle, or "pupil stop," is used routinely in UVES to provide a beam from calibration lamps (e.g., Th/Ar, flat field) similar in size to that from the telescope from an astronomical point source. Our I_2 exposures were taken with an under-sized pupil stop, i.e., a slightly smaller beam than usual was allowed into UVES, but our Th/Ar exposures used a slightly over-sized pupil stop. While these are the default settings for I_2 observations, strictly speaking our aim here is to treat the I_2 and Th/Ar exposures as similarly as possible so that any wavelength shifts between the two are appropriate to normal QSO observations where a slightly "oversize" pupil stop is used for both object and calibration exposures. However, we would not expect slight, circular vignetting/truncation of the beam to affect our results here. Indeed, subsequent iodine cell tests with UVES have shown any effect from the under-sized pupil stop to be very small, if present at all; these results will be presented in a forthcoming paper.

3. DATA REDUCTION AND ANALYSIS

The QSO flux was extracted using the standard pipeline recipes. Five bias and flat-field exposures were median filtered to produce master bias and flat-field corrections. The echelle order positions and overall spectrograph setup were derived from short-and-narrow slit exposures of quartz and Th/Ar lamps which were used to refine a physical model for the expected flux distribution within each order. In our exposures, the QSO flux had high enough signal/noise in each echelle order to allow the flux distribution itself to define its spatial profile for use as object weights in the subsequent optimal extraction. No redispersion of the spectra was performed after optimal extraction; each extracted echelle order retained its original wavelength dispersion as a function of pixel position. Rather than co-adding extracted QSO spectra, we treated each order of each exposure separately so that each I_2 (and accompanying Th/Ar) exposure gives a separate measurement of the Th/Ar wavelength calibration shifts for each order.

The UVES Common Pipeline Language (CPL) software package includes considerable improvements to the wavelength calibration process compared to previous UVES reduction pipelines. The Th/Ar line list is only a small subset of all known Th/Ar lines in the relevant wavelength range and was derived via an objective line selection algorithm detailed in Murphy et al. (2007). An even smaller subset is used in the final calibration, after the CPL pipeline removes those appearing too weak or strong/saturated in the individual Th/Ar spectra. The Th/Ar exposures were bias and (normalized) flat field corrected during the extraction. The extractions used the spatial weighting profile derived from the optimal extraction of the QSO flux from the corresponding I_2 exposure. This ensures that the same pixels, with the same weighting, contribute to both the QSO and Th/Ar spectrum and naturally avoid calibration errors from small tilts of the Th/Ar lines with respect to the CCD grid. A crude blaze correction was made using the flat-field spectral shape in each echelle order. To determine their centroid in the wavelength calibration process, the CPL pipeline fits Gaussian functions to the selected Th/Ar emission lines. The Gaussian model includes an underlying linear (rather than just constant offset) continuum level; this reduces centroiding errors induced by other nearby emission lines or other sources of background slopes, e.g., residual blaze function (Murphy et al. 2007).

The wavelength calibration residuals around the default two-dimensional fourth-order polynomial wavelength solution had an rms of $\sim$ 30–40 m s^{-1}, similar to that found from the unbinned Th/Ar exposures by Murphy et al. (2007). We also performed wavelength calibration using higher order polynomials and we study the effect of this in Section 4.1.

To perform the wavelength recalibration using the iodine lines, we used a method similar to that used in Griest et al. (2010). A well-measured iodine cell absorption spectrum taken elsewhere is convolved with a Gaussian to give it the same resolution as the iodine lines in our QSO spectra. It is then multiplied by an overall normalization and shifted in wavelength by an amount that gives the smallest possible χ^2 in the difference between the convolved iodine spectrum and the QSO spectra. Care is taken in the continua fitting as discussed in Griest et al. (2010), since the iodine lines cover nearly the entire

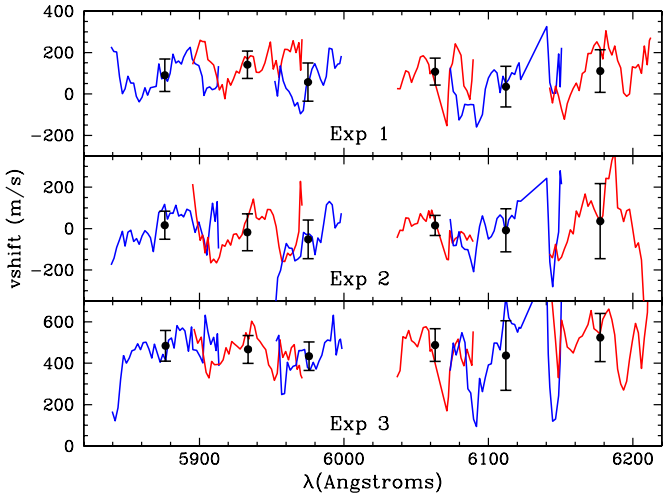

Figure 1. Shift in m s^{-1} needed to bring the Th/Ar VLT-UVES calibration in line with the iodine spectrum. This figure shows results for the three exposures orders of the UVES upper "u" CCD chip, with blue and red colors alternating for each echelle order. The black dots show the weighted average of the shifts in each order, with error bars showing the average 1σ fit error for each order.

(A color version of this figure is available in the online journal.)

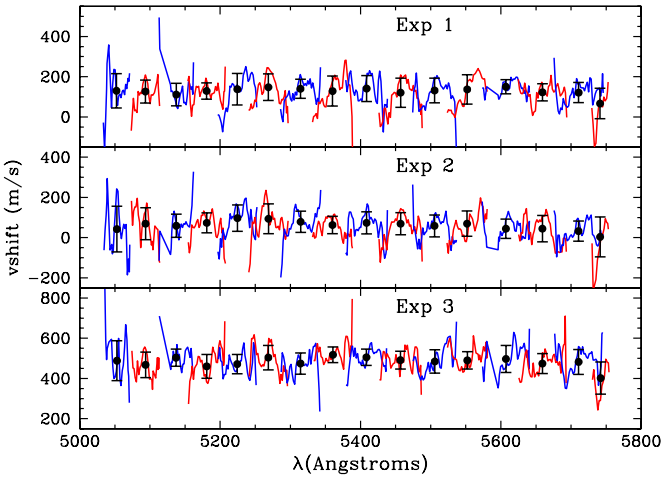

Figure 2. Same as the previous figure, but for the lower "l" CCD chip.

(A color version of this figure is available in the online journal.)

spectrum. For the reference iodine spectra, we tried both the Marcy and Butler (Butler et al. 1996; Marcy 2008, unpublished) FTS spectrum of the Keck HIRES iodine cell done at KPNO with a resolving power, $R = 170{,}000$ and a signal/noise of 700 pixel^{-1}, and the UVES iodine cell calibration spectrum,[3] performed at 70°C, with a spectral resolution 0.020 cm^{-1} (which implies $R > 1{,}000{,}000$ throughout the effective I_2 wavelength range). Besides the difference in resolution and a single shift in the absolute scale, the resulting calibration shifts were fairly similar using the two different reference spectra. For UVES iodine cell data, it is clearly more appropriate to use the UVES FTS iodine cell spectrum so we will only present results obtained using this spectrum.

4. RESULTS

The result of our analysis is a wavelength-dependent velocity shift $v_{\rm shift}(\lambda)$ between the iodine cell value, which is presumed to be correct, and the Th/Ar value output by the UVES pipeline software,

$$\lambda_{\rm I}(\lambda) = \lambda_{\rm ThAr}(\lambda) + v_{\rm shift}(\lambda), \quad (1)$$

where there is one such velocity shift function for each echelle order of each exposure. We use the iodine cell calibration as the standard since it has a much higher density of lines and because the QSO and the iodine light follow the same optical path, have the same instrument illumination, and are simultaneous. Additional evidence in support of the superiority of the iodine cell wavelength scale and discussion of whether $v_{\rm shift}$ arises primarily from the extraction software or from optical distortion inside the spectrograph are given below. In fact, it is not important to our work that the FTS iodine spectrum be absolutely correct, since we only care about relative shifts across an individual exposure, and perhaps shifts over time. And since the extraction of the Th/Ar spectra was performed using the same object weights as that of the QSO flux, the I_2 and Th/Ar spectra are treated as similarly as possible in the reduction process, meaning that any wavelength distortions derived should be driven by optical distortions rather than any deficiencies of the reduction pipeline.

The fit for the $v_{\rm shift}$ calibration offset is affected by the size of the wavelength bin used in the comparison, with a larger bin giving a smaller formal fit error but less resolution on the wavelength scale over which calibration errors occur. As a compromise, we use a bin of 350 km s^{-1} or 6 Å at 5500 Å. We translate these wavelength calibration shifts into velocity using $v_{\rm shift} = c\Delta\lambda/\lambda$ and display the result for each exposure in Figures 1 and 2.

Considering each order from each iodine exposure separately, we began by continuum fitting the exposure and masking the data that fall under strong quasar absorption lines and data near the edges of the order where signal/noise dropped to <8 pixel^{-1}. Considering the remaining data as one large wavelength bin, we performed a simultaneous fit for three variables: the overall normalization multiplication factor to the continuum, the Gaussian convolution kernel, and the overall wavelength shift. The wavelength offset found this way is in some sense the average offset for the entire order. We then held the Gaussian convolution sigma and normalization factor fixed for the whole order and fit for the wavelength calibration shifts in the smaller wavelength bins across the order. We fit using a bin size of 350 km s^{-1} and report the value of the bin at the average wavelength value within the bin. The bins overlap which means the wavelength calibration has effectively gone through a smoothing filter of 350 km s^{-1}.

One sees from Figures 1 and 2 that there are two distinct types of velocity shifts. First, there is an exposure-dependent overall average calibration shift which varies from less than 100 m s^{-1} in exposure 2, to around 500 m s^{-1} in exposure 3. Second, there are intra-order velocity shifts around the overall average shift ranging in size from around 100 m s^{-1} up to around 400 m s^{-1} within each exposure and within each echelle order. Both types of shifts were also seen in the Keck HIRES iodine cell data (Griest et al. 2010), but with considerably larger amplitude. Exposures 1 and 2 have an overall average shift of around 100 m s^{-1}, while exposure 3, taken on the next day, is off by about 500 m s^{-1}. It is important to note that the overall average velocity shifts between exposures do not affect fine-structure constant work significantly; velocity shifts which vary with wavelength—i.e., effects which would shift one absorption feature with respect to another at a different wavelength—are

[3] http://www.eso.org/sci/facilities/paranal/instruments/uves/tools

Table 2
Means[a] and Standard Deviations[a] of Calibration Shifts

Exposure	Chip	Unweighted	Unweighted Corrected[b]	Weighted and Clipped[c]	Weighted and Clipped Corrected[b,c]
1	l	118 ± 76	115 ± 73	133 ± 58	123 ± 52
2	l	45 ± 86	42 ± 87	63 ± 69	53 ± 70
3	l	487 ± 75	483 ± 85	485 ± 60	475 ± 67
1	u	116 ± 138	116 ± 129	107 ± 87	102 ± 73
2	u	0 ± 137	0 ± 130	−5 ± 87	−9 ± 70
3	u	477 ± 174	475 ± 172	499 ± 115	495 ± 105

Notes.
[a] All numbers are in m s^{-1}.
[b] Each pixel has a correction added before calculation. See the text.
[c] The mean is calculated using the error bars as weights and then recalculated after throwing out points more than 3σ from the mean.

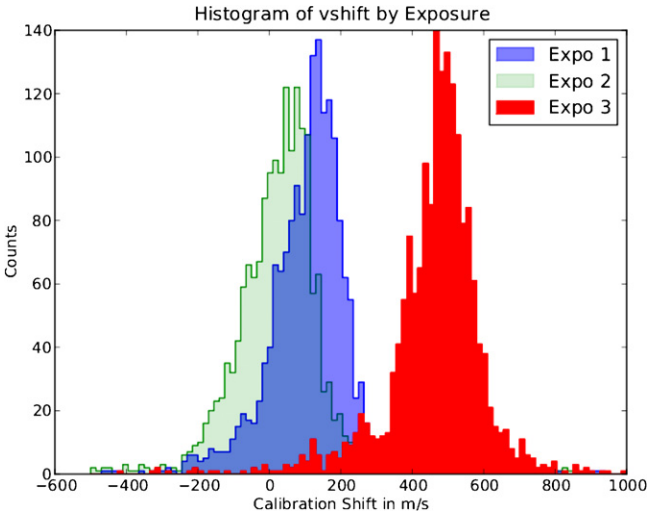

Figure 3. Histograms of shifts from the three I_2 exposures. Exposure 1 is plotted in blue (in the middle), exposure 2 in green (on the left), and exposure 3 in red (on the right).

(A color version of this figure is available in the online journal.)

most important (e.g., Webb et al. 1999; Murphy et al. 2009). Thus, we are most interested in the relative intra-order shifts within each exposure of typically 100 m s^{-1} and occasionally as high as 500 m s^{-1}. The cause of these intra-order shifts is not completely understood, but some possibilities will be discussed below.

Another way of visualizing the velocity shifts in Figures 1 and 2 is to plot the shift distributions. These are shown in Figure 3 which are just histograms of the shifts for each of the exposures. The shift from each fine wavelength bin is given equal weight in the figure, which, if normalized, can therefore be interpreted as a sort of probability of finding a shift of that value. We use this histogram in this way below when we investigate the effect these shifts might have on measurements of $\frac{\Delta\alpha}{\alpha}$. Of course, the shift values for nearby pixels are strongly correlated due to our smoothing, but this is not important for how we use these distributions below. We give the values of the means and standard deviations for these histograms in Table 2. Again, it is only the width (sigma) of each histogram that is relevant for fine-structure constant work, and not the overall average shift which is the histogram mean.

As discussed above, the exposure-dependent, overall average velocity shifts are of the magnitude one may expect from errors in the position of the QSO in the spectrograph slit. These types of shifts could also be caused by grating shifts, temperature/pressure drifts, etc. In preliminary work using the UVES iodine cell on exposures toward bright stars, we do find that varying the position of the star within the slit can give shifts between Th/Ar and iodine calibrations of around 1500 m s^{-1}, making this a likely contributor.

Next, we would like to explore the possibility that there is a relatively constant intra-order distortion that repeats for each order and is constant between exposures. If the intra-order distortion pattern for a given object exposure can be well approximated from a subsequent I_2 exposure, either of the QSO or of a nearby bright star, then one can correct the Th/Ar wavelength scale of the former, i.e., a sort of calibration transfer function can be established and applied. We are interested in the effect of wavelength calibration on $\frac{\Delta\alpha}{\alpha}$,

$$\Delta\alpha/\alpha \propto \Delta v_{ij}/c, \quad (2)$$

where Δv_{ij} is the velocity difference *between* two lines, i and j within the one spectrum.

Examination of Figures 1 and 2 might give one the impression that there is a pattern of intra-order velocity offsets that repeats in each echelle order. To test this hypothesis, we overlaid all the echelle orders of each exposure on their common CCD pixel scale and then averaged them in bins of 100 pixels. We plot the mean and standard deviation in each bin in Figures 4(a)–(c) and 5(a)–(c). The dashed lines show the average over all bins. These figures thus provide the average intra-order distortion for a given exposure. We do this separately for each exposure since the distributions of shifts shown in Figure 3 show large variation between the exposures. We also treat the UVES upper, "u," chip orders separately from the UVES lower, "l," chip orders. Thus, we have a total of six figures.

Examination of these figures shows a weak pattern, especially for the "u" chip. We see a roughly linear rise in $v_{\rm shift}$ of around 200 m s^{-1} starting around pixel number 1000 and ending around pixel 2900, where there is a sharp drop of over 100 m s^{-1}. The "l" chip figures show smaller overall variance and while exposures 1 and 2 show some rise over the first half of the pixels, the amplitude is smaller than for the "u" chip. Exposure 3 of the "l" chip does not seem to have any pattern of deviation. Examination of the standard deviations listed in Table 2 confirms these impressions, especially that most of the variance comes from the "u" chip. This is also clear in Figures 1 and 2 where the larger "u" chip variances are evident.

As stated above, the purpose of looking for patterns is to find a correction that could be applied to all exposures. Modeling the "u" chip deviation as a linear rise of 200 m s^{-1} over pixels between 1000 and 2900, we can subtract this line from each of the exposures and recalculate the means and standard deviations. The results of this "correction" are displayed in Table 2. We

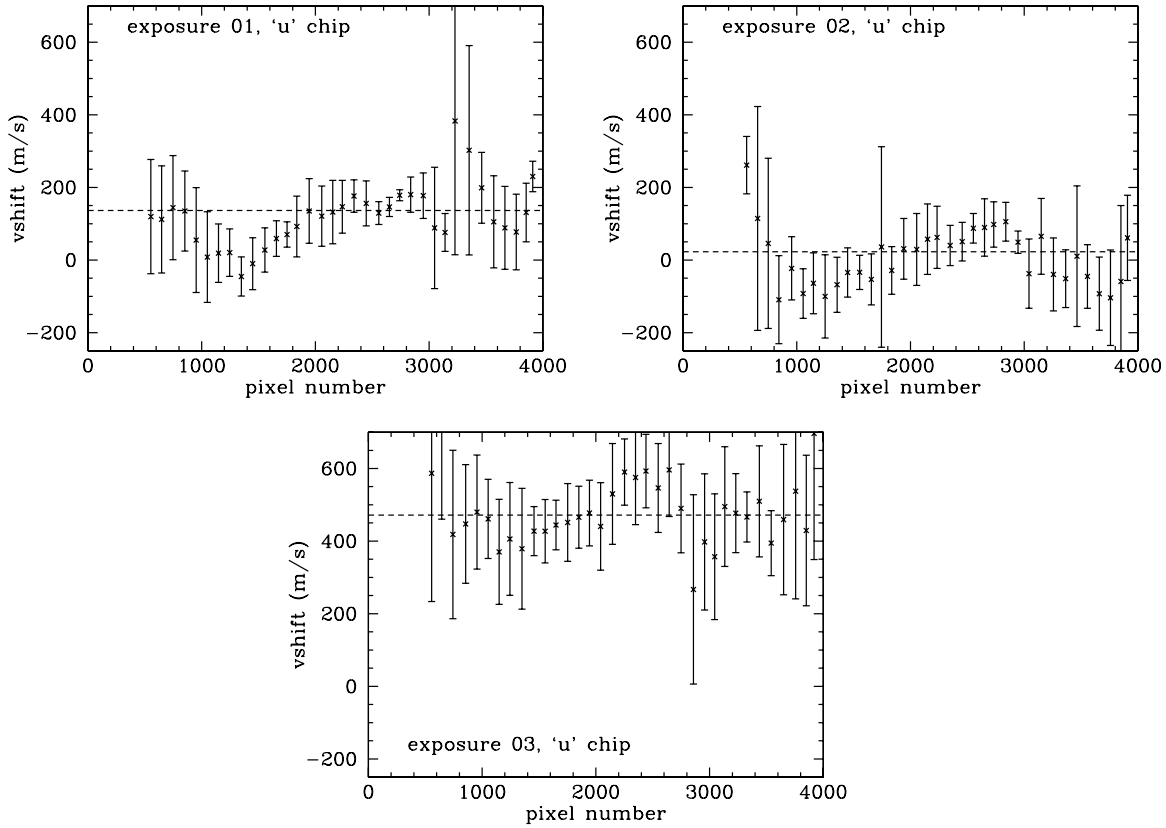

Figure 4. Average over echelle orders of calibration shifts for the "u" (upper) chip as a function of pixel number. The echelle average calibration shift in m s^{-1} at each position bin is plotted on the ordinate. The standard deviation in the bin of each calibration shift is plotted as the error bar. The dashed line shows the average over all bins.

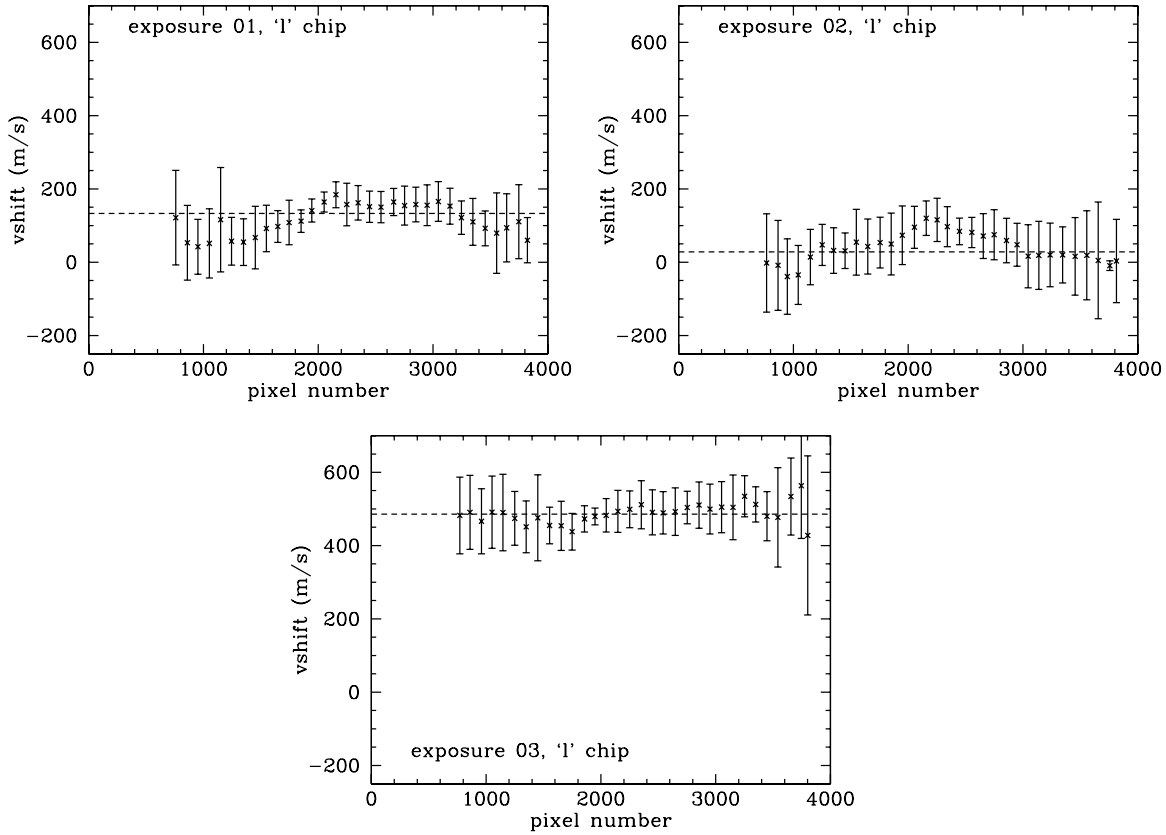

Figure 5. Same as the last figure, but for the lower "l" chip.

only expect this to decrease the standard deviations for the "u" chip, but show the "l" chip results also for completeness. We find a small decrease in standard deviations, especially for the weighted and sigma-clipped means and standard deviations. For example, the variance in exposure 1 "u" chip goes from 87 m s^{-1} to 73 m s^{-1}; exposure 2 and exposure 3 also drop their sigma values by around 10 m s^{-1}. We had hoped for more improvement, but with only three iodine exposures, we view this work as illustrative rather than conclusive. More data are needed in order to further explore the size and constancy of this type of correction.

4.1. Effect of Degree of Polynomial in Th/Ar Calibration

We would like to find the source of the intra-order wavelength miscalibrations discovered above, especially whether they come from the spectrograph and/or telescope themselves or from something in the extraction and calibration software. In this section, we consider the extent to which the polynomial fit for the wavelength solution contributes to wavelength scale error. Thus, besides the standard spectrum extraction using a fourth degree polynomial fit for the Th/Ar wavelength solution, we also extracted and calibrated the spectra using fifth and sixth degree polynomials. Figure 6 shows the differences between these Th/Ar solutions versus wavelength. The thick black lines show fourth degree minus fifth degree, thin blue lines show fourth minus sixth degree, and dashed red lines show fifth minus sixth. The upper panel shows the upper CCD "u" chip, and the lower panel shows the "l" chip. We see that there is substantial disagreement between these wavelength solutions especially for the upper CCD and near the edges of the echelle orders. For the upper chip, disagreements of 30–40 m s^{-1} are typical with 100 m s^{-1} not uncommon. For the lower chip, agreement is typically within 10–20 m s^{-1}, with outliers mostly near the trailing edge of the orders. Note that it is not clear that using a sixth-order polynomial does a better job, since the disagreement between fifth and sixth order (dashed red line) can be appreciable.

Next, we recalibrated these spectra using the iodine cell method. Figure 7 shows the velocity shifts needed to bring the Th/Ar calibrations in line with the iodine spectrum. The black lines are for the fourth degree polynomial fit and are the same shifts plotted in Figures 1 and 2, while the thinner red lines are for the sixth degree polynomial fit. Note that the distortions in the wavelength scale from polynomial fitting (differences between the red and black lines) are substantially smaller than the total intra-order distortions, especially for the lower "l" chip where the red lines are mostly on top of the black lines. This shows that polynomial fitting errors are not the primary source of the intra-order distortions.

We also compared the absolute wavelength scales found by the iodine method, $\lambda_I(\lambda)$ in Equation (1), for the fourth, fifth, and sixth degree polynomial fits. These agreed with each other exceedingly well, with rms differences between the fourth and sixth degree fits of 1 m s^{-1} or less for the lower "l" CCD chip, and rms differences of 5 m s^{-1} or less for the upper "u" chip. This is a nice confirmation of the robustness of our iodine fitting method, since this high level of agreement obtained even very near the edges of the echelle orders where the different polynomial fits disagreed greatly.

Thus, we have several interesting conclusions. First, we see from Figure 6 that the polynomial extraction algorithm can make a significant contribution to wavelength miscalibration, especially in the upper "u" CCD and most especially near the edges

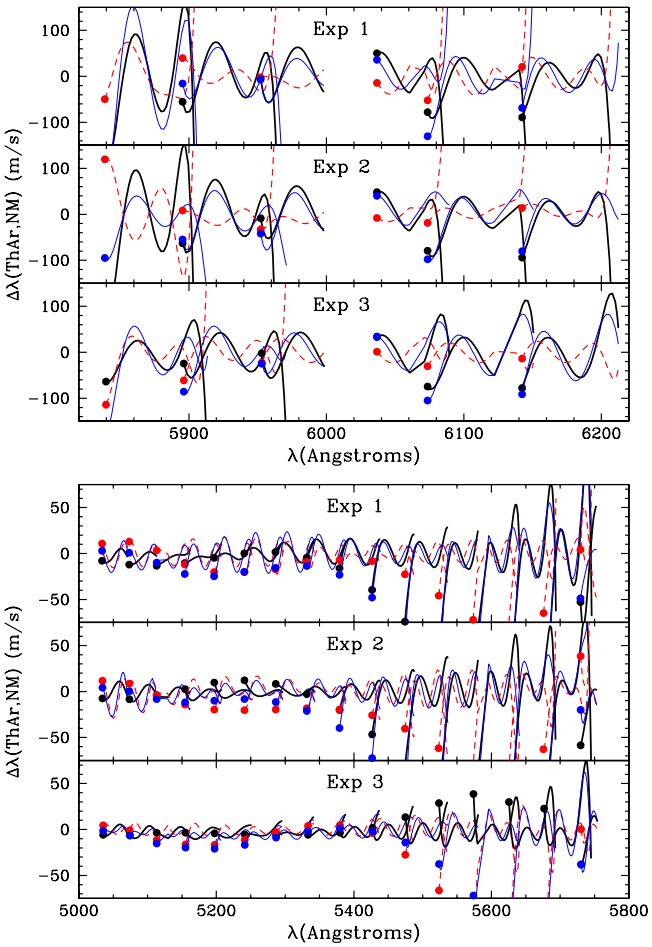

Figure 6. Differences in Th/Ar wavelength solutions for orders occurring on the upper "u" CCD chip (upper panel) and lower "l" CCD chip (lower panel). The thick solid black lines show the difference in wavelength scale between extractions done with a fourth-order polynomial and a fifth-order polynomial. The thin solid blue lines show the fourth order minus the sixth order, and the dashed red lines show the fifth order minus the sixth order. The beginning of each order is shown by a big dot and exposure number is labeled. Note the different scales on the upper and lower chips.

(A color version of this figure is available in the online journal.)

of the echelle orders, where velocity shifts of order 70 m s^{-1} are common. Second, there is little evidence that a sixth-order polynomial does a better job than a fourth-order polynomial, since in both cases the robust iodine cell recalibration shows similar size miscalibrations. Thus, we caution against the use of lines near the edges of the echelle orders calibrated only using Th/Ar. Third, the overall contribution to the miscalibration variance of the polynomial fitting is small compared to other contributions. Thus, better treatment of wavelength fitting in spectra extraction will not cure the main source of intra-order wavelength miscalibration we are finding.

4.2. Possible Causes for the Intra-order Distortions

While more work is clearly needed for understanding the ultimate cause(s) of the velocity shifts (both the overall shifts between exposures and the intra-order distortions within individual exposures), this will probably require a larger data set with higher spectral signal/noise and/or spanning a range in several parameters such as time and telescope pointing. Nevertheless, we briefly discuss some possible causes for the intra-order distortions between the iodine and Th/Ar calibrations.

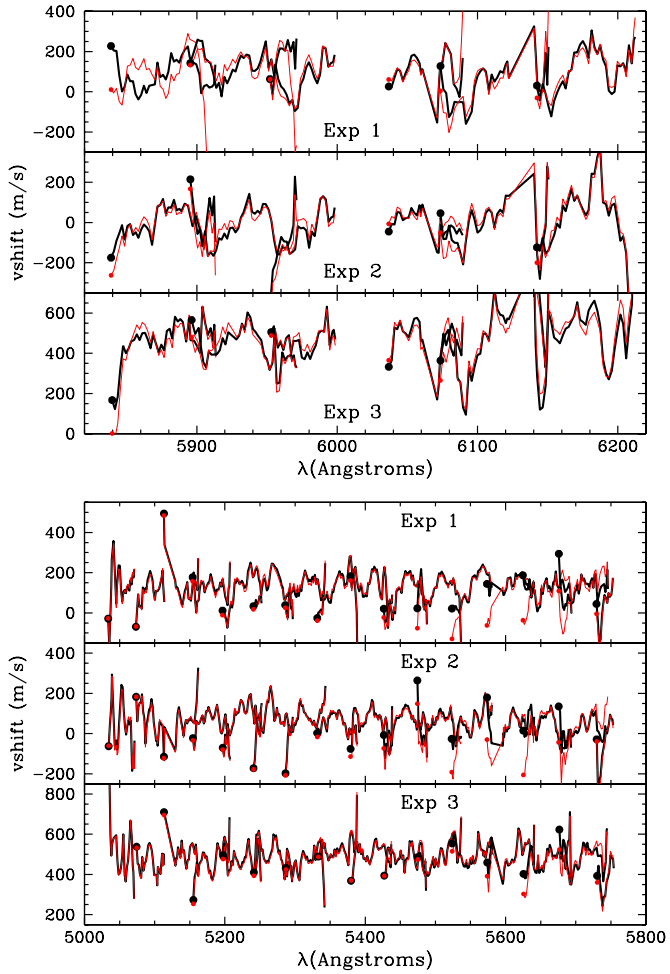

Figure 7. Velocity shift needed to bring the Th/Ar UVES calibration in line with iodine spectrum. The upper panel shows the results for the three exposures for the upper "u" CCD chip, and the lower panel shows the lower "l" chip. The thick black lines show results for the fourth degree polynomial fit, while the thin red lines show the sixth degree fit. The beginning of each echelle order is marked with a large dot.

(A color version of this figure is available in the online journal.)

First, for Keck/HIRES, Griest et al. (2010) cited a known misalignment between the Keck telescope optical axis and that of HIRES (Suzuki et al. 2003) as a probable cause for the regular shape of the intra-order distortions from order to order. The misalignment causes differential vignetting between the telescope beam and that of HIRES (and, therefore, the Th/Ar beam). While we are unaware of a similar misalignment in UVES, it remains possible that similar differential vignetting is responsible for the intra-order distortions found here. In general and despite the use of the simple pupil stop in UVES, the science object and Th/Ar calibration light do not follow the same optical path, and so we regard a subtle differential effect of similar, or even subtler nature to be responsible.

However, other simpler effects may also be suspected at first. The very similar shape of the intra-order distortions across many orders in HIRES, and the weaker but broadly similar tendency revealed in Figure 4 and, to a lesser extent, Figure 5 for UVES, brings to mind the blaze function of echelle spectrographs. For example, one may worry that the centroiding of Th/Ar emission lines is systematically shifted in opposite directions either side of the order center, thereby producing an intra-order distortion which, broadly speaking, was similar across all orders. However, this possibility can be ruled out: the slope produced by the blaze is too small, as shown by the following simple considerations. In selecting Th/Ar lines best used for calibrating UVES, Murphy et al. (2007) measured the velocity shift between two Gaussian fits to each line, one with a constant offset continuum, the other with a sloping continuum. It was found that a background slope of 0.01 $(\mathrm{km\,s^{-1}})^{-1}$ in relative line intensity resulted in a $\sim$160 $\mathrm{ms^{-1}}$ shift in the line centroid if only a constant offset continuum was fitted. If the blaze function of UVES is not normalized out of the Th/Ar spectra, then the background intensity will drop by a factor of 2 over half the free spectral range (FSR) either side of the center of each order. UVES's FSR is $\sim$3000 $\mathrm{km\,s^{-1}}$. Thus, the average slope of the inner half of the blaze function is $\sim \pm 0.5/(0.5 \times 3000\,\mathrm{km\,s^{-1}}) = 3 \times 10^{-4}\,(\mathrm{km\,s^{-1}})^{-1}$ or, since it is curved, the maximum slope will certainly be $\lesssim 1 \times 10^{-3}$. This would translate to a line shift of only $160\,\mathrm{m\,s^{-1}} \times 1 \times 10^{-3}/0.01 = 16\,\mathrm{m\,s^{-1}}$. This upper limit is an order of magnitude below the intra-order distortions we observe.

The above blaze effect will not appear in our UVES Th/Ar calibration because the Gaussian fits to the Th/Ar lines had a sloped continuum. Also, our Th/Ar extractions involve a crude blaze correction; even if this did not reliably remove all blaze effects, the resulting line shifts would be smaller than the above calculation indicates. For example, the very broad spectral shape of the quartz lamp which provides the flat-field light will remain in our CPL-reduced Th/Ar spectra (and the I_2 spectra), but the above argument demonstrates that such a broad background spectral shape will have negligible effects and cannot explain the intra-order distortions we find. Similar blaze effects probably play little role in the HIRES results of Griest et al. (2010) because the data reduction pipeline which provided their main results (HIRES REDUX by Jason X. Prochaska) uses a sloped continuum. They also used another pipeline (MAKEE by Tom Barlow) that used a constant offset continuum, but found similar results. That is, any effect from the blaze function in the Griest et al. results will be small by comparison to the intra-order distortions measured there.

Recently, Wilken et al. (2010) compared the wavelength scales established from a laser frequency comb (LFC) and a standard Th/Ar lamp in one echelle order of the HARPS spectrograph on the ESO 3.6 m telescope. The LFC revealed periodic artifacts in the physical pixel size and/or sensitivity from the CCD manufacturing process. By appropriately correcting the sensitivity of every 512th pixel, the wavelength calibration residuals were substantially improved. They also found distortions between this LFC calibration and that from the Th/Ar lamp. Perhaps the CCD manufacturing defects cause this distortion and contribute to the intra-order distortions we find for UVES. This seems unlikely because the Th/Ar lines are distributed randomly and very sparsely across the CCD grid, so very few (if any) Th/Ar lines straddle a pixel with a manufacturing defect. In fact, the Th/Ar–LFC distortions found by Wilken et al. seem similar in shape and magnitude to those we find for UVES between different Th/Ar solutions using different polynomial degrees; compare Figure 6 with their Figure 4 (blue line).

Finally, we note that a similar method for discovering shifts in the Th/Ar calibration of UVES has been demonstrated by Molaro et al. (2008a). They compared the solar spectrum reflected from asteroids with a laboratory FTS solar spectrum to establish the wavelength scale of UVES and compare it with the Th/Ar solution. First, it is interesting to note that they only

find small (10–50 m s^{-1}) average velocity shifts for different exposures, possibly indicating that accurate centroiding of the asteroids within the 0.″5 wide slit was achieved. However, only the line cores of a few solar absorption features per echelle order were utilized, so it is difficult to assess whether the intra-order distortions we find here are reflected in the results of Molaro et al. (2008a).

5. EFFECT ON $\frac{\Delta\alpha}{\alpha}$

As stated in the introduction, wavelength calibration errors of the magnitude presented in this paper are unimportant for most astronomical work. In this section, we wish to address the question of whether or not calibration errors such as we are finding can make a difference in experiments looking for changes in $\frac{\Delta\alpha}{\alpha}$. In order to proceed, we need an estimate of the magnitude of $\frac{\Delta\alpha}{\alpha}$ we wish to be sensitive to. There are at least two possible sources for this number: first, $\frac{\Delta\alpha}{\alpha} = (-5.7 \pm 1.1) \times 10^{-6}$, which is the most robust claimed detection of $\frac{\Delta\alpha}{\alpha}$ (Murphy et al. 2001a, 2001b, 2003, 2004), and second, there are several claimed limits on $\frac{\Delta\alpha}{\alpha}$ near $\frac{\Delta\alpha}{\alpha} < 1 \times 10^{-6}$ (Chand et al. 2004; Srianand et al. 2004; Levshakov et al. 2006, 2007; Molaro et al. 2008b; cf. Murphy et al. 2008). Thus, the question we would like to ask is to see whether the UVES wavelength calibration errors discussed above can alone give rise to estimates of $\frac{\Delta\alpha}{\alpha}$ in the 1×10^{-6} to 5×10^{-6} range.

Naively, one might expect the calibration errors of 200 m s^{-1} to 500 m s^{-1} we found above to give rise to spurious detections of $\frac{\Delta\alpha}{\alpha}$ of order 1×10^{-6}. If α was different in the past, the velocity shift of an absorption line from the lab value due to changing α can be found from

$$v_j = v_0 + \left(\frac{\Delta\alpha}{\alpha}\right) x_j, \quad x_j = -2cq_j\lambda_{0j}, \tag{3}$$

where j numbers the atomic transitions that are being compared, v_0 is a constant offset (degenerate with the system redshift), the x_j are constants that depend only on the wavelength λ_0 of the transition, and the q_j characterize the sensitivity of each transition to a change in $\frac{\Delta\alpha}{\alpha}$. For transitions of interest in QSO absorption work, these q-values range in magnitude from around 20 cm^{-1} to 2000 cm^{-1} (Porsev et al. 2007), giving rise to velocity shifts of a few meters per second up to around 100 m s^{-1} (for a value of $\frac{\Delta\alpha}{\alpha} = -5.7 \times 10^{-6}$). Thus, for individual transitions, the sizes of the wavelength calibration errors found above are of the order of or larger than the sizes of the signal expected from a changing α.

However, the value of $\frac{\Delta\alpha}{\alpha}$ obtained does not depend upon just one transition, but is always a comparison of two or more transitions. Thus, an overall velocity shift of 500 m s^{-1} as seen in exposure 3 above is not relevant as long as comparisons are not done across different exposures. Figures 1 and 2 show that the relative shift across one exposure is substantially smaller than the overall shift. In addition, if the calibration shift error is random, and equally likely to be negative as positive, then it can be removed by averaging over many transitions and many lines of sight. Potential problems do exist if the distribution of relative shifts is not random, or if the sizes of the errors are large enough that a good measurement requires too many transitions or too many lines of sight. Thus, we wish to perform some mock experiments using the above distributions of calibration shifts to see what the effect on $\frac{\Delta\alpha}{\alpha}$ would be.

In an actual experiment, a value of $\frac{\Delta\alpha}{\alpha}$ is estimated by doing a large joint fit of the Voigt line profiles, the system redshifts, and the possible velocity offset due to $\frac{\Delta\alpha}{\alpha}$. In our Monte Carlo mock experiments, we try to calculate a value of $\frac{\Delta\alpha}{\alpha}$ using the UVES VLT data, but without measuring any actual absorption lines. Instead of using the fitted system redshifts to find velocity offsets, we use the wavelength calibration offsets given by the fine-binned (blue and red) lines in Figures 1 and 2 and add these to the lab values of λ_0 in Equation (3).

The basic method is as follows. We first choose a random redshift in the range $z = 0.2$ to $z = 3.7$ and calculate the wavelengths of the 23 atomic transitions that were studied in Murphy et al. (2003). We define $N_{\rm tran}$, the number of these 23 transitions that fall at wavelengths for which we have iodine wavelength calibration. We require at least $N_{\rm min}$ transitions and show our results as a function of this $N_{\rm min}$ (a typical value is $N_{\rm min} = 4$, and we do not find any cases with $N_{\rm tran} > 9$). For each such transition, we shift its wavelength by an amount given by the fine-binned (blue or red) line from one of the exposures in Figures 1 and 2. We then perform a fit of Equation (3) for $\frac{\Delta\alpha}{\alpha}$ and its error. This counts as one absorption system, and we repeat this procedure $N_{\rm sys}$ times, averaging the values of $\frac{\Delta\alpha}{\alpha}$ obtained. We consider values of $N_{\rm sys}$ ranging from $N_{\rm sys} = 143$, the number of systems used in Murphy et al. (2004), to $N_{\rm sys} = 1$, the value when only one system in one QSO is being analyzed. The above procedure constitutes one Monte Carlo experiment. We repeat the experiment many times to find an average value of $\frac{\Delta\alpha}{\alpha}$ and its standard deviation (measured by the variance of $\frac{\Delta\alpha}{\alpha}$ for the many experiments).

We present resulting average values of $\frac{\Delta\alpha}{\alpha}$ along with their standard deviations as a function of $N_{\rm sys}$ and $N_{\rm min}$ in Table 3 for 200,000 mock experiments. The table shows results for $N_{\rm sys} = 143$ and $N_{\rm sys} = 1$. Note that one expects the standard deviation in $\frac{\Delta\alpha}{\alpha}$ to simply scale as $N_{\rm sys}^{-1/2}$, which is close to what we find in Table 3. Thus, we will use this scaling from now on and only report Monte Carlo experiments for $N_{\rm sys} = 1$.

Besides using the actual wavelength calibration errors above, we also ran several Monte Carlo simulations using two simple models of the calibration offsets. The results of these simple models are also reported in Table 3. For the first model, we used a Gaussian random velocity offset with a standard deviation equal to 91 m s^{-1}. For the second, we modeled the velocity offsets as a sine function with amplitude equal to $\pi/2$ times the standard deviation of the velocity offsets for one of the exposures above, and with a wavelength of about one echelle order. For this case, we found the results did not depend strongly on the sine wavelength. As seen in Table 3, the results for $\sigma(\frac{\Delta\alpha}{\alpha})$ are quite similar for all three exposures and for the Gaussian and sine function models.

Table 3 shows several interesting things. First in all cases when $N_{\rm min} = 2$, both the mean calibration offset and standard deviation in $\frac{\Delta\alpha}{\alpha}$ are substantially larger than expected from a simple $1/\sqrt{N_{\rm tran}}$ scaling. We think this is due to occasional cases where there are very few transitions found, but these lie close together in $x_j = -2cq_j\lambda_j$. Since $\frac{\Delta\alpha}{\alpha}$ is basically the slope in Equation (3), a small Δx offset can result in a very large slope and therefore a large error in $\frac{\Delta\alpha}{\alpha}$. It takes just a few such cases to greatly increase the standard deviation. A lesson here may be to not use systems in which very few transitions can be compared. For example, in the alkali doublet method (e.g., Bahcall et al. 1967; Varshalovich et al. 2000, etc.) two transitions that are close

Table 3
Monte Carlo Results[a] for Mean and Standard Deviation of $\frac{\Delta\alpha}{\alpha}$

Exposure	$N_{\rm min}$	$\frac{\Delta\alpha}{\alpha}$ Mean/10^{-6}	$\sigma/10^{-6}$ for $N_{\rm sys}=1$	$\sigma/10^{-6}$ for $N_{\rm sys}=143$
1	2	1.74	41.6	3.57
1	4	0.53	5.21	0.443
1	6	−0.041	3.28	0.267
2	2	−1.68	44.7	3.74
2	4	0.330	6.41	0.540
2	6	0.297	3.36	0.279
3	2	1.02	58.9	4.83
3	4	0.706	6.67	0.548
3	6	0.245	3.43	0.280
Gaussian	2	−0.502	115	...
Gaussian	4	−0.080	11.2	...
Gaussian	6	−0.012	4.23	...
Sine	2	−1.78	104	...
Sine	4	−3.13	12.6	...
Sine	6	−0.308	4.64	...

Note. [a] Only transitions within the iodine cell coverage are included from 200,000 realizations of $N_{\rm sys}=1$.

together in wavelength are compared, so this method would be sensitive to intra-order distortions. More generally, even for $N_{\rm min}=4$ and $N_{\rm min}=6$, we find the errors dropping more quickly with N than $1/\sqrt{N}$.

Next, we note that the results for all three exposures and for the Gaussian and sine function error models are quite consistent, especially when one takes into account that the standard deviation of velocity offsets for exposure 1 is slightly smaller than for the other exposures. Also as expected, the large overall velocity shift for exposure 3 had no effect.

If we restrict ourselves to the $N_{\rm min}=6$ column and consider $N_{\rm sys}=143$, we see that the systematic error introduced to a many multiplet measurement of $\frac{\Delta\alpha}{\alpha}$ is around 0.28×10^{-6}, significantly smaller than the statistical error of 1.16×10^{-6} stated in Murphy et al. (2003, 2004). We do note that Murphy et al. (2003, 2004) used the Keck HIRES spectrograph and not the VLT-UVES instrument.

An important problem with the above results is that the value of $\frac{\Delta\alpha}{\alpha}$ and its standard deviation depends strongly on $N_{\rm tran}$, the number of transitions compared in each system, and that no cases were found with $N_{\rm tran}>9$. This latter fact is because the results above only included lines that overlapped with our iodine cell coverage. Thus, $N_{\rm tran}$ found in our Monte Carlo experiments are artificially lower than in an actual experiment, which typically has more spectral coverage. Since the value of $\sigma(\frac{\Delta\alpha}{\alpha})$ drops quickly with an increase in $N_{\rm tran}$, we also expect an actual experiment to find smaller deviations than the ones we report. We find this low value of $N_{\rm tran}$ to be especially true for certain values of z, where very few interesting lines fall within our iodine cell coverage. Our attempt to get around this by setting a minimum number of transitions, $N_{\rm min}$, was partially successful, but Table 3 shows strong dependence on $N_{\rm min}$. Even more clearly, we see this in Table 4 where the values of sigma of $\frac{\Delta\alpha}{\alpha}$ depend on $N_{\rm tran}$ substantially more strongly than $1/\sqrt{N_{\rm tran}}$. We note that when $N_{\rm tran}$ is specified in the table, exactly $N_{\rm tran}$ transitions are compared, while when $N_{\rm min}$ is specified all cases that have $N_{\rm tran}\geqslant N_{\rm min}$ are used.

To remedy this situation, we need to somehow estimate the calibration offsets in regions of the spectra where we do not have iodine cell coverage. We attempt to do this by replicating the calibration offsets from the regions where we measure them to all the other spectral regions where interesting transitions occur; i.e., we assume that the distributions of shifts illustrated in Figures 1 and 2 apply to all wavelengths. We then repeat the Monte Carlo experiments above.

Table 4
Standard Deviation[a] of $\frac{\Delta\alpha}{\alpha}$ from Wavelength Calibration Errors as a Function of the Number of Transitions

$N_{\rm tran}$	Percentage of Realizations	Exposure 1: $\sigma/10^{-6}$	Gaussian: $\sigma/10^{-6}$
2	20.7%	228	91.4
3	29.7%	30.3	44.0
4	18.7%	8.61	11.2
5	11.7%	5.90	5.00
6	10.7%	3.34	4.17
7	6.3%	3.10	3.73
8	1.3%	3.36	3.60
9	1.0%	2.59	3.18

Note. [a] For transitions that occur within the iodine cell coverage region of the spectrum, and for 200,000 realizations of $N_{\rm sys}=1$.

Results of these simulations are shown in Figure 8 and in Table 5. Now, we find few systems with less than 10 transitions and many with around 18. The values of $\sigma(\frac{\Delta\alpha}{\alpha})$ for low values $N_{\rm min}$ are similar to those found in the iodine-coverage-only Monte Carlos, again depending very strongly on $N_{\rm min}$ (or $N_{\rm tran}$). However, for larger values of $N_{\rm min}$, $\sigma(\frac{\Delta\alpha}{\alpha})$ stabilizes and approaches the expected $1/\sqrt{N_{\rm tran}}$ behavior as $N_{\rm min}$ increases.

The strong dependence of $\sigma(\frac{\Delta\alpha}{\alpha})$ on $N_{\rm min}$ is interesting and suggests that the standard lore that says it is better to use transitions in the same echelle order may not be true. The wavelength calibration errors we found above exist even within single echelle orders. Thus, it may be more robust to measure or limit $\frac{\Delta\alpha}{\alpha}$ using transitions that are well separated in x; the extra "lever arm" may be advantageous in reducing scatter.

Overall, the large σ's found at small $N_{\rm tran}$ imply that due to wavelength calibration errors it may be dangerous to attempt to measure $\frac{\Delta\alpha}{\alpha}$ using only a few transitions in one or two systems. Until better understanding is found as to the source of these calibration errors, it is probably important to average the errors away by using many transitions in many absorption systems.

We also see from Figure 8 that the mean and standard deviation for all three exposures agree well and that the three

Table 5
Monte Carlo Results[a] for Mean and Standard Deviation of $\frac{\Delta\alpha}{\alpha}$

$N_{\rm min}$	Exposure 1: Mean/10^{-6}	Exposure 1: $\sigma/10^{-6}$	Gaussian: Mean/10^{-6}	Gaussian: $\sigma/10^{-6}$
2	−0.018	81.2	0.185	91.6
4	−0.101	4.99	−0.036	5.64
6	−0.064	2.59	−0.028	3.04
8	−0.051	2.00	−0.006	2.38
10	−0.042	1.71	−0.005	2.03
15	−0.029	1.30	0.004	1.59
20	0.153	1.05	0.007	1.35

Note. [a] All of the 23 transitions falling between 3000 Å and 10500 Å are included (see the text), for 200,000 realizations of $N_{\rm sys} = 1$.

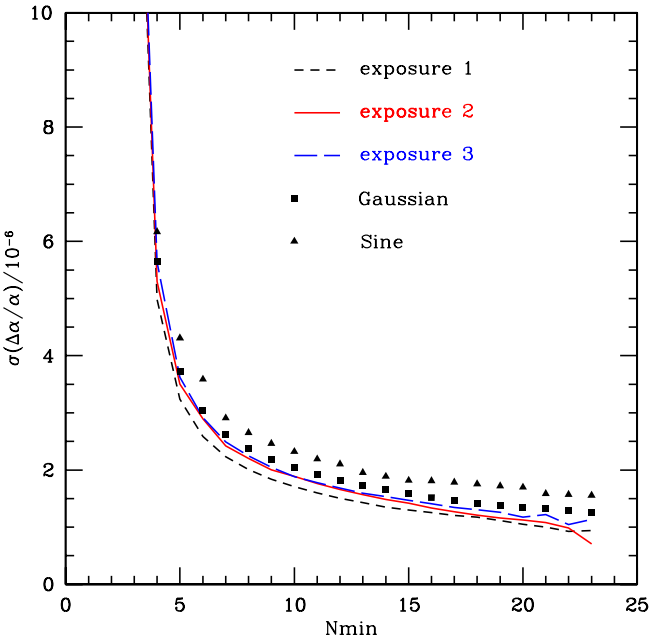

Figure 8. Scaling of $\sigma(\frac{\Delta\alpha}{\alpha})$ with $N_{\rm min}$, the minimum number of transitions allowed in a system. This is for full wavelength coverage between 3000 Å and 10,500 Å, with repeated calibration errors. 200,000 Monte Carlo realizations were used with $N_{\rm sys} = 1$.

(A color version of this figure is available in the online journal.)

experimentally determined measurements of $\sigma(\frac{\Delta\alpha}{\alpha})$ are well modeled by a Gaussian (or sine function) model with the same velocity standard deviation. Thus, it seems that the error in $\frac{\Delta\alpha}{\alpha}$ caused by this wavelength calibration is completely specified by just the standard deviation of the velocity offsets. In order to quantify this, we ran a suite of simulations using various values of $\sigma(v)$. We found we could fit all the results for $\sigma(\frac{\Delta\alpha}{\alpha})$ with a fairly simple formula:

$$\sigma\left(\frac{\Delta\alpha}{\alpha}\right) = 7.5 \times 10^{-8} C_{\rm Nt} \frac{\sigma(v)}{(N_{\rm sys} N_{\rm tran})^{\frac{1}{2}}}, \quad (4)$$

where $\sigma(v)$ is in m s^{-1}, and $C_{\rm Nt} \approx 1$ (to within 10%) for $N_{\rm tran} \geqslant 8$ and $C_{\rm Nt} = 21$ for $N_{\rm tran} = 2$, $C_{\rm Nt} = 5.1$ for $N_{\rm tran} = 3$, $C_{\rm Nt} = 1.7$ for $N_{\rm tran} = 4$, $C_{\rm Nt} = 1.3$ for $N_{\rm tran} = 5$, and $C_{\rm Nt} = 1.1$ for $N_{\rm tran} = 6$ or $N_{\rm tran} = 7$. The simulations were done with our ansatz for full wavelength calibration between 3000 Å and 10,500 Å.

6. CONCLUSIONS

We tested the accuracy of the wavelength calibration of the VLT-UVES spectrograph by recalibrating the standard Th/Ar calibration pipeline output using spectra taken though the UVES iodine cell. We found several types of miscalibration: first, an exposure-dependent overall average velocity shift that is probably mostly due to the position of the QSO within the spectrograph slit. Repositioning of the spectrograph gratings and pressure/temperature drifts inside the spectrograph may also contribute to these velocity shifts. These overall average shifts range up to 500–600 m s^{-1}, but do not affect fine-structure constant measurements as long as comparisons between absorption features are only performed within the same spectrum.

Second, and more importantly, we found intra-order calibration shifts of up to several hundred meters/seconds that occur within the same spectrum and within each echelle order. These can affect measurement of the fine-structure constant. We investigated several possible causes for these shifts. We explored the effect of the degree of the polynomial used in the Th/Ar calibration and found a velocity dispersion of 20–40 m s^{-1} due to this. This is several times smaller than the total dispersion we find in the velocity measurements, so the main effect we are finding is not due to the degree of the Th/Ar calibration polynomial. In fact, we found that the iodine cell recalibration of extractions using different degree polynomials allowed us to regain the same absolute wavelength scale to an accuracy of better than 5 m s^{-1}, thus showing the robustness of our iodine recalibration method. We considered several other possible causes for the intra-order shifts and showed that spectrograph blaze function and related possibilities were unlikely. Thus, we conclude that most likely there are unknown hardware-related systematic errors within UVES and/or the VLT responsible for these shifts. We noticed some weak patterns in the shift as a function of CCD pixel and attempted a correction based upon these patterns. This correction was not very successful, so we conclude that additional data and analysis are required to discover the cause and potential fixes for these wavelength scale shifts. We note that it is important look for such a correction, since if the intra-order distortion pattern for a given object exposure could be well approximated from a subsequent I_2 exposure, either of the QSO or of a nearby bright star, then one could correct the Th/Ar wavelength scale of the former, i.e., a sort of calibration transfer function could be established and applied.

We next explored the effect of these shifts on determination of or limits on the value of the fine-structure constant. Using our measured shifts, we performed Monte Carlo experiments and found that the effect of the intra-order shifts is well modeled by a Gaussian dispersion in wavelength calibration with a

magnitude of around 80–120 m s^{-1}. We found that the effect on $\frac{\Delta\alpha}{\alpha}$ depended strongly on the number of lines being compared within the spectrum, with the use of a small number of lines resulting in larger than expected errors. Thus, until a correction to these intra-order wavelength miscalibrations is found, we recommend against focusing on comparison between pairs of lines or the use of spectra which contain only a few lines. We summarized the results of our Monte Carlo experiments in a fitting formula (Equation (4)), which should be useful in estimating the effect of these (or similar) wavelength calibration problems on future fine-structure work.

J.B.W. and K.G were supported in part by the U.S. Department of Energy under grant DE-FG03-97ER40546. M.T.M. thanks the Australian Research Council for a QEII Research Fellowship (DP0877998).

REFERENCES

Bahcall, J. N., Sargent, W. L. W., & Schmidt, M. 1967, ApJ, 149, L11
Butler, R. P., Marcy, G. W., Williams, E., McCarthy, C., Dosanjh, P., & Vogt, S. S. 1996, PASP, 108, 500
Chand, H., Srianand, R., Petitjean, P., & Aracil, B. 2004, A&A, 417, 853
D'Odorico, S., et al. 2000, Proc. SPIE, 4005, 121
Griest, K., Whitmore, J. B., Wolfe, A. M., Prochaska, J. X., Howk, J. C., & Marcy, G. W. 2010, ApJ, 708, 158
Johnson, J. A., et al. 2006, ApJ, 647, 600
Konacki, M. 2009, in IAU Symp. 253, Transiting Planets, ed. F. Pont, D. D. Sasselov, & M. J. Holman (Cambridge: Cambridge Univ. Press), 141
Levshakov, S. A., Centurión, M., Molaro, P., D'Odorico, S., Reimers, D., Quast, R., & Pollmann, M. 2006, A&A, 449, 879
Levshakov, S. A., Molaro, P., Lopez, S., D'Odorico, S., Centurión, M., Bonifacio, P., Agafonova, I. I., & Reimers, D. 2007, A&A, 466, 1077
Molaro, P., Levshakov, S. A., Monai, S., Centurión, M., Bonifacio, P., D'Odorico, S., & Monaco, L. 2008a, A&A, 481, 559
Molaro, P., Reimers, D., Agafonova, I. I., & Levshakov, S. A. 2008b, Eur. Phys. J. Spec. Top., 163, 173
Murphy, M. T., Tzanavaris, P. T, Webb, J. K., & Lovis, C. 2007, MNRAS, 378, 221
Murphy, M. T., Webb, J. K., & Flambaum, V. V. 2003, MNRAS, 345, 609
Murphy, M. T., Webb, J. K., & Flambaum, V. V. 2004, VizieR Online Data Catalog, 734, 50609
Murphy, M. T., Webb, J. K., & Flambaum, V. V. 2008, MNRAS, 384, 1053
Murphy, M. T., Webb, J. K., & Flambaum, V. V. 2009, Mem. Soc. Astron. Ital., 80, 833
Murphy, M. T., Webb, J. K., Flaumbaum, V. V., Churchill, C. W., & Prochaska, J. X. 2001a, MNRAS, 327, 1236
Murphy, M. T., Webb, J. K., Flambaum, V. V., Dzuba, V. A., Churchill, C. W., Prochaska, J. X., Barrow, J. D., & Wolfe, A. M. 2001b, MNRAS, 327, 1208
Osterbrock, D. E., Waters, R. T., Barlow, T. A., Slanger, T. G., & Cosby, P. C. 2000, PASP, 112, 733
Porsev, S. G., Koshelev, K. V., Tupitsyn, I. I., Kozlov, M. G., Reimers, D., & Levshakov, S. A. 2007, Phys. Rev. A, 76, 052507
Srianand, R., Chand, H., Petitjean, P., & Aracil, B. 2004, Phys. Rev. Lett., 92, 121302
Suzuki, N., Tytler, D., Kirkman, D., O'Meara, J. M., & Lubin, D. 2003, PASP, 115, 1050
Varshalovich, D. A., Potekhin, A. Y., & Ivanchik, A. V. 2000, in AIP Conf. 506, X-Ray and Inner-Shell Processes, ed. R. W. Dunford et al. (Argonne, IL: Argonne National Laboratory)
Webb, J. K., Flambaum, V. V., Churchill, C. W., Drinkwater, M. J., & Barrow, J. D. 1999, Phys. Rev. Lett., 82, 884
Wilken, T., et al. 2010, MNRAS, 405, L16